

The Simons Observatory: Studies of Detector Yield and Readout Noise From the First Large-Scale Deployment of Microwave Multiplexing at the Large Aperture Telescope

Thomas P. Satterthwaite ^{a,b}, Zeeshan Ahmed ^{b,c}, Kyuyoung Bae ^d, Mark Devlin ^e, Simon Dicker ^e, Shannon M. Duff ^f, Daniel Dutcher ^g, Saianeesh K. Haridas ^e, Shawn W. Henderson ^{b,c}, Johannes Hubmayr^f, Bradley R. Johnson ^h, Anna Kofman ^e, Jack Lashner ⁱ, Michael J. Link ^f, Tammy J. Lucas ^f, Alex Manduca ^e, Michael D. Niemack ^{j,k}, John Orłowski-Scherer ^e, Tristan Pinsonneault-Marotte ^{b,c}, Max Silva-Feaverⁱ, Suzanne Staggs ^g, Eve M. Vavagiakis^{j,l}, Yuhan Wang ^g, and Kaiwen Zheng ^g

^aDepartment of Physics, Stanford University; Stanford, CA 94305; USA

^bKavli Institute for Particle Astrophysics and Cosmology; Stanford, CA 94305; USA

^cSLAC National Accelerator Laboratory; Menlo Park, CA 94025; USA

^dUniversity of Colorado Boulder; Boulder, CO, 80309; USA

^eDepartment of Physics and Astronomy, University of Pennsylvania; Philadelphia, PA 19104; USA

^fQuantum Sensors Division, National Institute of Standards and Technology; Boulder, CO, 80305; USA

^gJoseph Henry Laboratories of Physics, Princeton University; Princeton, NJ 08542; USA

^hDepartment of Astronomy, University of Virginia; Charlottesville, VA 22904; USA

ⁱWright Laboratory, Department of Physics, Yale University; New Haven, CT 06520; USA

^jDepartment of Physics, Cornell University; Ithaca, NY 14853; USA

^kDepartment of Astronomy, Cornell University; Ithaca, NY 14853; USA

^lDepartment of Physics, Duke University; Durham, NC 27708; USA

ABSTRACT

The Simons Observatory is a new ground-based cosmic microwave background experiment, which is currently being commissioned in Chile’s Atacama Desert. During its survey, the observatory’s small aperture telescopes will map 10% of the sky in bands centered at frequencies ranging from 27 to 280 GHz to constrain cosmic inflation models, and its large aperture telescope will map 40% of the sky in the same bands to constrain cosmological parameters and use weak lensing to study large-scale structure. To achieve these science goals, the Simons Observatory is deploying these telescopes’ receivers with 60,000 state-of-the-art superconducting transition-edge sensor bolometers for its first five year survey. Reading out this unprecedented number of cryogenic sensors, however, required the development of a novel readout system. The SMuRF electronics were developed to enable high-density readout of superconducting sensors using cryogenic microwave SQUID multiplexing technology. The commissioning of the SMuRF systems at the Simons Observatory is the largest deployment to date of microwave multiplexing technology for transition-edge sensors. In this paper, we show that a significant fraction of the systems deployed so far to the Simons Observatory’s large aperture telescope meet baseline specifications for detector yield and readout noise in this early phase of commissioning.

Keywords: Cosmic microwave background, Simons Observatory, cosmology, microwave frequency multiplexing, SMuRF

Corresponding author: Thomas P. Satterthwaite
Email: tpsatt@stanford.edu

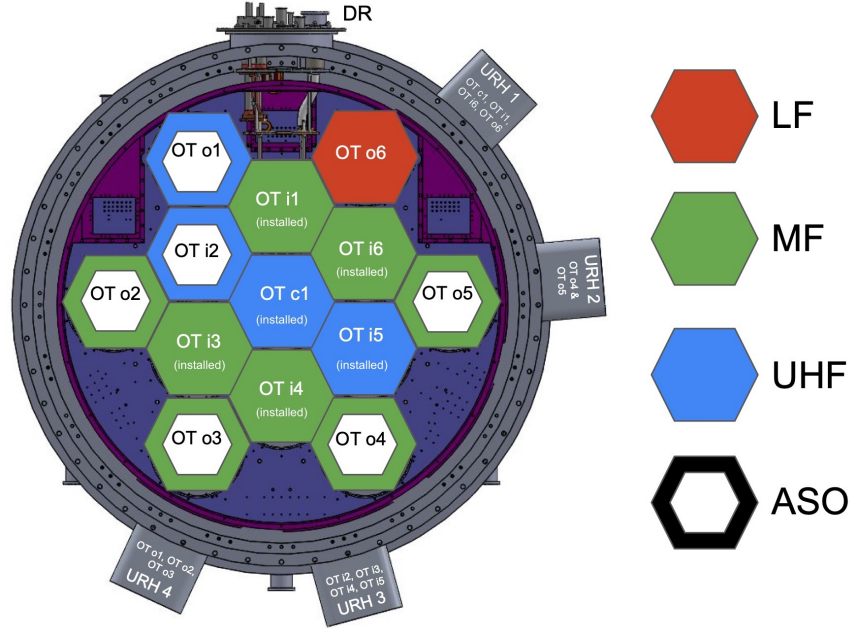


Figure 1: Rear-view schematic showing the positions of the LAT receiver’s optics tubes (OTs), with low-frequency (LF), mid-frequency (MF), and ultra-high-frequency (UHF) OTs labelled. The LF OT and those slated for the Advanced Simons Observatory (ASO) upgrade have not yet been installed. Positions of the dilution refrigerator (DR), which provides cooling, and the universal readout harnesses (URHs), which support the DC lines and RF coaxial channels, are also shown. Credit: Bob Thornton/University of Pennsylvania LATR team.

1. INTRODUCTION

The Simons Observatory is a cosmic microwave background (CMB) experiment which is currently being commissioned at an elevation of 5,200 m on Cerro Toco in Chile’s Atacama Desert. The experiment presently consists of three 0.5 m refracting small aperture telescopes (SATs) and a single 6 m Crossed Dragone large aperture telescope (LAT), with bandpasses ranging from 27 to 280 GHz.¹ The SATs will map 10% of the sky targeting $2 \mu\text{K}$ -arcmin map noise in 90 and 150 GHz bands with the aim of searching for *B*-mode polarization to constrain cosmic inflation models. The LAT will map 40% of the sky targeting $6 \mu\text{K}$ -arcmin map noise in 90 and 150 GHz bands with the aims of constraining cosmological parameters, studying the Universe’s large-scale structure via weak gravitational lensing, and constraining the sum of the masses of neutrinos. The Simons Observatory collaboration has constructed all four telescopes on Cerro Toco, and the LAT is expected to achieve first light in early 2025.

Constructing the Simons Observatory requires fabricating and deploying 60,000 state-of-the-art superconducting transition-edge sensor (TES) bolometers. These TESs are split across the four telescopes with roughly 10,000 in each SAT and 30,000 in the LAT.²³ The detectors are deployed in universal focal-plane modules (UFMs), each of which contains up to 1,756 TESs (of which up to 1,720 are optically coupled) and 28 multiplexer chips.⁴ These multiplexer chips use microwave superconducting quantum interference device (SQUID) multiplexing (μmux) in order to achieve multiplexing factors reaching 910 and enable high-density readout; this is a dramatic improvement over previous iterations of time- and frequency-division multiplexing technologies which have each been able to reach a maximum factor of 68 when deployed for CMB science.⁵⁶⁷ This has been enabled by the large-scale fabrication of TESs and microwave SQUIDs, and by the development of the SLAC Microresonator RF (SMuRF) electronics, a novel signal transduction and readout system.⁸⁹¹⁰

In μmux , each TES is inductively coupled to a SQUID which is in turn coupled to a microwave frequency resonator such that the change in TES current induced by observed signals perturbs the resonator’s frequency. The SMuRF system provides the integrated electronics for serving the tones which drive and track the resonators,

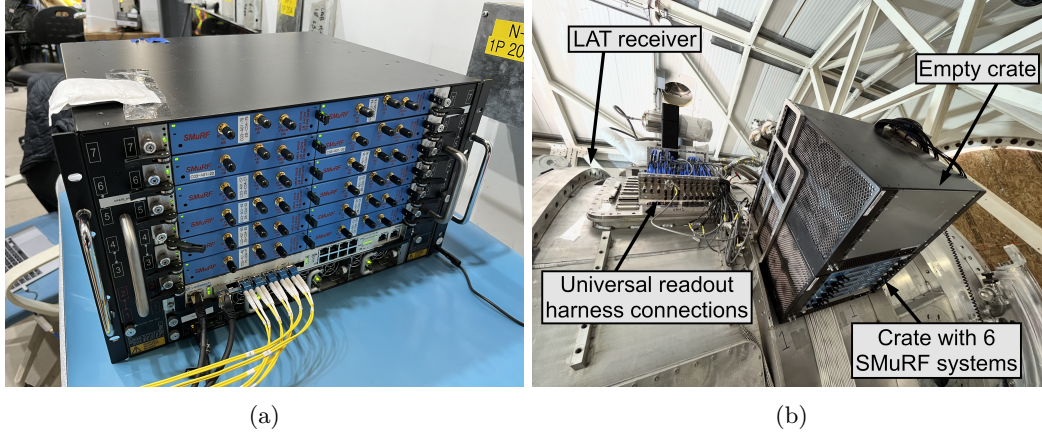


Figure 2: (a) One crate containing six SMuRF systems on a test bench in the Simons Observatory high bay lab facility on Cerro Toco, Chile. (b) Two crates, one populated with six SMuRF systems and the other empty, mounted to the LATR (without fiber, RF coaxial, and DC cables installed).

the flux ramp signal which linearizes the SQUID response, and the DC signal which biases the TESs. This therefore enables the deployment, control, and data acquisition of μ mux technology at scale.

The construction of the Simons Observatory has been the largest deployment to date of a μ mux system for astronomy; previous deployments of μ mux at MUSTANG-2 and the Keck Array, for example, have read out 215 and 528 detectors, respectively.¹¹¹² As 7 UFM have been deployed to each SAT and 18 have been deployed to the LAT, a commensurate number of SMuRF systems, with each one able to provide the warm readout electronics for a single UFM, have also been deployed. As such, an important part of ensuring the readiness of these systems and their UFM for CMB observation is measuring the detector channel yield and readout noise, and ensuring that these statistics match required performance specifications. The following section of this paper discusses ongoing work towards this end for the Simons Observatory’s LAT.

2. READOUT COMMISSIONING

The deployment of the LAT’s optics tubes (OTs) to the cryogenic LAT receiver (LATR) has occurred in phases. In mid-2023, two OTs (identified as OTi1 and OTi6) were installed and capped at 4 K. In early 2024, four more OTs (identified as OTc1, OTi3, OTi4, and OTi5) were installed, and all six OTs were capped at 300 K. The positions of these OTs are shown in Figure 1. Each OT contains three UFM for a current total of 18 UFM containing more than 30,000 TESs.³ Along with each deployment of UFM, a commensurate number of SMuRF systems have also been installed in the LAT to provide the warm readout electronics for the detector modules. One crate containing six SMuRF systems is shown in Figure 2a. As of early 2024, four such crates, each containing between three and six SMuRF systems, have been mounted to the exterior of the LATR, as shown in Figure 2b, so that they are able to corotate with the receiver as the elevation structure rotates. The next planned personnel deployment to the LAT site is scheduled for mid-2024, when we will continue the commissioning tasks which require in-person operations.

As the LAT’s mirrors are expected to be delivered in early 2025, each optics tube is currently capped at 300 K with an aluminum plate. Nonetheless, characterization of the dark performance of the UFM and SMuRF systems during this phase of commissioning provides valuable information and statistics about detector and readout performance. As we carry out these activities, we seek to meet baseline specifications for the Simons Observatory’s operation, including a detector yield in excess of 70%, with the goal of reaching 80%, and readout noise equivalent current below the level of $65 \text{ pA}/\sqrt{\text{Hz}}$, with the goal of reaching $45 \text{ pA}/\sqrt{\text{Hz}}$. Meeting these specifications will enable us to meet the Simons Observatory’s science goals.¹

Since the departure of the LATR instrument team in early 2024, we have seen a few fixable hardware-related issues with the telescope’s readout system. During the re-installation of OT OTi6 in early 2024, there was an accidental swap involving its cold coaxial cabling, so this OT’s UFM cannot currently be read out. This OT

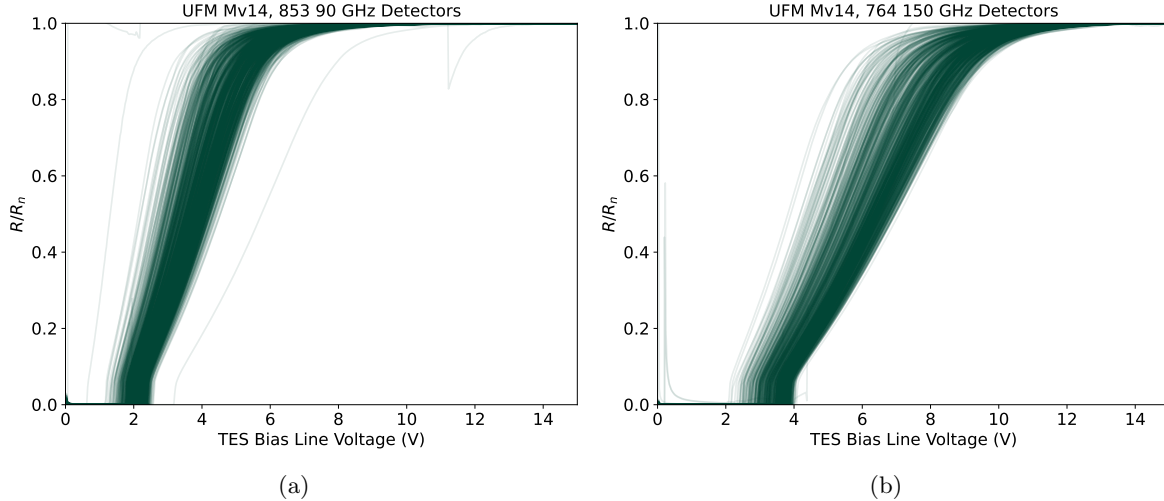


Figure 3: Curves showing TES resistance (relative to normal resistance) versus bias line voltage for the (a) 90 GHz and (b) 150 GHz detectors of a sample UFM (Mv14).

was, however, operational in mid-2023 when it was capped at 4K, so we are able to present results from that phase of commissioning. Since early 2024, we have also seen a few SMuRF hardware-related issues. On the SMuRF system reading out UFM Mv28, we find that the RF tone power being applied is inadequate due to an RF tone generation hardware problem. We plan to replace the relevant SMuRF part in mid-2024. On the SMuRF systems reading out UFMs Mv21 and Mv24, the SMuRF DC cables appear to be inadequately engaged. We have seen and fixed this issue in the past, so we plan on correcting it during our next trip to the site by reseating and securing, or possibly replacing, the connectors. Because UFMs Mv21, Mv24, and Mv28 were all deployed to the LATR in mid-2023, we are still able to present results from their initial commissioning, when their OTs were capped at 4K. Finally, we have also seen hardware issues relating to the DC and low-frequency biasing systems of the SMuRF systems which read out UFMs Mv34 and Mv49. We plan to correct these issues by replacing the relevant SMuRF parts in mid-2024, however we are not yet able to present any commissioning data from these systems.

2.1 Detector Yield

We measure detector yield by determining the number of detectors which exhibit visible, smooth transitions from normal to superconducting states. We determine this total yield by using SMuRF to locate and track the resonators to which the detectors are coupled, and to measure the detectors' responses to input electrical power. Note that, as defined, this total yield is the net effect of detector-only and readout-only losses.

This process first requires determining the correct power at which to send the probe tones which interrogate each resonator. To do this, we can adjust the tone power itself, as well as the attenuations of the upconverters and downconverters which come before and after the signal enters and returns from the cryostat, respectively. Leaving the tone power fixed, as it strongly influences the readout noise which is discussed in the following section, we have determined these attenuations by finding the combination which minimizes the streamed noise level from the detectors. With the probe tone power properly optimized, shifts in the frequencies of these resonators, as would be induced by detector signals, can then be tracked via SMuRF's closed-loop tracking algorithm.

Once resonances have been located and tracked, we characterize the detectors by taking $I-V$ curves. These measure the response of each TES (as read out through the SQUIDs to which they are coupled) as a range of voltages are applied to their bias lines, which have an average resistance of about $16\text{ k}\Omega$, and through the TESs, which have a normal resistance (R_n) of about 7 to $9\text{ m}\Omega$ and are shunted by resistors of approximately $400\text{ }\mu\Omega$. This creates curves as shown in Figure 3 (scaled to R/R_n), showing the transition between normal and superconducting behavior. A detector is then considered part of the yield if it demonstrates a visible, smooth transition from a flat normal region to a superconducting state as determined by basic quality cuts. We have taken these curves for 16 UFMs deployed to the LAT, and results are summarized in Table 1.

Table 1: Detector yield from 16 UFM and SMuRF systems.

Optics Tube Identifier	UFM Identifier	Detector Yield (#)	Detector Yield (%)
OTi1	Mv28	1496	85.2
	Mv24	1516	86.3
	Mv21	1423	81.0
OTi6	Mv25	1629	92.8
	Mv11	1306	74.4
	Mv26	1493	85.0
OTi3	Mv13	1057	60.2
	Mv20	1589	90.5
OTi4	Mv14	1617	92.1
	Mv32	1555	88.6
OTi5	Uv42	1503	85.6
	Uv31	1504	85.6
	Uv47	1557	88.7
OTc1	Uv46	1437	81.8
	Uv39	1542	87.8
	Uv38	1300	74.0

Due to the hardware issues discussed in Section 2 which affect two SMuRF DC and low-frequency biasing systems, results are not presented from their associated UFM (identified as Mv34 and Mv49). Due to the cold coaxial cabling, RF tone generation, and DC cable engagement issues discussed in the same section, results presented for UFM Mv11, Mv21, Mv24, Mv25, Mv26, and Mv28 are from studies performed prior to the early 2024 deployment, when their OTs were capped at 4 K. The procedure was, however, the same as that used for the ten UFM which were surveyed later in 2024, when their OTs were capped at 300 K. We expect that the change in optical loading has a limited effect on the detector yield as determined using this method, so the yield would therefore be consistent for 300 K caps.

We see that the detector yield of 15 of the presented UFM and SMuRF systems is in excess of 70% of deployed TESs. We find these results promising as they satisfy the baseline performance requirement, and 13 UFM satisfy the goal requirement of 80% yield. Furthermore, 14 UFM show detector yields which are within 10% of pre-deployment screening numbers, with potential gains available when the remaining detector modules are assessed and further optimized.¹³¹⁴ Work is ongoing to understand and potentially correct the insufficient yields of the UFM which do not meet the goal specification. UFM Mv11’s yield is known to be low because of a problem with a TES bias line on the module, and we plan to repair this issue. For other UFM, insufficient yield could be due to missing or collided resonators, to detectors which are not tracking well due to SQUID properties, or to damaged wire bonds or traces.

2.2 Readout Noise

Given that the LAT’s TESs are not currently optically loaded by the sky, when they are normal (off-transition), noise is dominated by the quadrature sum of their Johnson noise and the readout noise.⁴ We can therefore infer the readout noise equivalent current by subtracting the known contribution of Johnson noise from the median spectral white noise level that we compute between 10 and 30 Hz. With normal TESs, the low-frequency limit of the Johnson noise current spectral density is given by:

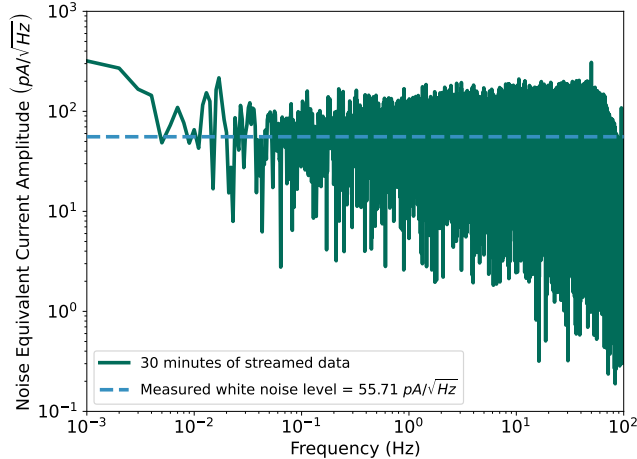


Figure 4: Amplitude spectral density of 30 minutes of streamed data from a sample detector whose white noise level is close to the overall median. Peak at 50 Hz is due to the frequency of Chilean AC power. Amplitude spectral density is cut off at 100 Hz due to the Nyquist sampling of the readout filter which is applied. This also causes the roll-off towards higher frequencies.

$$\text{NEI}_{\text{Johnson}} = \sqrt{\frac{4k_B (T_S R_S + T_{\text{TES}} R_{\text{TES}})}{(R_S + R_{\text{TES}})^2}}$$

Where T_S is the temperature of the TES’s shunt resistor (which we approximate to be the bath temperature, T_{Bath}), R_S is the resistance of said shunt resistor, T_{TES} is the TES’s temperature, R_{TES} is the TES’s normal resistance, and k_B is the Boltzmann constant.

For OTs OTc1, OTi3, OTi4, and OTi5, we inferred readout noise by recording 30 minute-long streams sampled at 200 Hz with the detectors normal. These detector conditions were achieved by setting the bath temperature higher than the TESs’ critical temperatures (typically $T_c \approx 165$ mK and $T_{\text{Bath}} \approx 220$ mK).¹³¹⁴ A sample amplitude spectral density of data from one detector taken using this method is shown in Figure 4. We then calculated and subtracted off the Johnson noise using this bath temperature for T_S and T_{TES} , and the per-UFM median R_{TES} as measured prior to deployment to Chile.¹³¹⁴

Due to the cold coaxial cabling, RF tone generation, and DC cable engagement issues discussed in Section 2, we were not able to use this procedure for OTs OTi1 and OTi6 which contain UFM’s Mv11, Mv21, Mv24, Mv25, Mv26, and Mv28. Instead, we present results from late 2023 when the systems were operational. In this test, the detectors were made normal by driving saturation current through each of the UFM’s TES bias lines in order to induce sufficient heating. This brought T_{TES} above the detectors’ critical temperatures, which were measured prior to deployment to Chile. We could then approximate and subtract off the Johnson noise using the per-UFM median values of these critical temperatures and of R_{TES} , which was also measured prior to deployment. We intend to re-characterize the readout noise of these UFM’s using longer streams and a raised bath temperature after the hardware issues are addressed this summer.

Results for the calculated readout noise from 16 UFM’s are shown in Figure 5. Due to the SMuRF DC and low-frequency biasing system issues discussed in Section 2, results are not presented from UFM’s Mv34 and Mv49. For the other UFM’s, we see that there is not a significant difference between the calculated readout noise levels as given by driving saturation current through the TESs’ bias lines (as denoted by asterisks in the figure) and that given by raising the bath temperature. We find that 15 of the surveyed UFM’s show median readout noise levels below $65 \text{ pA}/\sqrt{\text{Hz}}$. This is a promising result as it shows performance consistent with the baseline specification for science operation. For UFM Uv47, which shows an anomalously high readout noise level, we are investigating this issue.

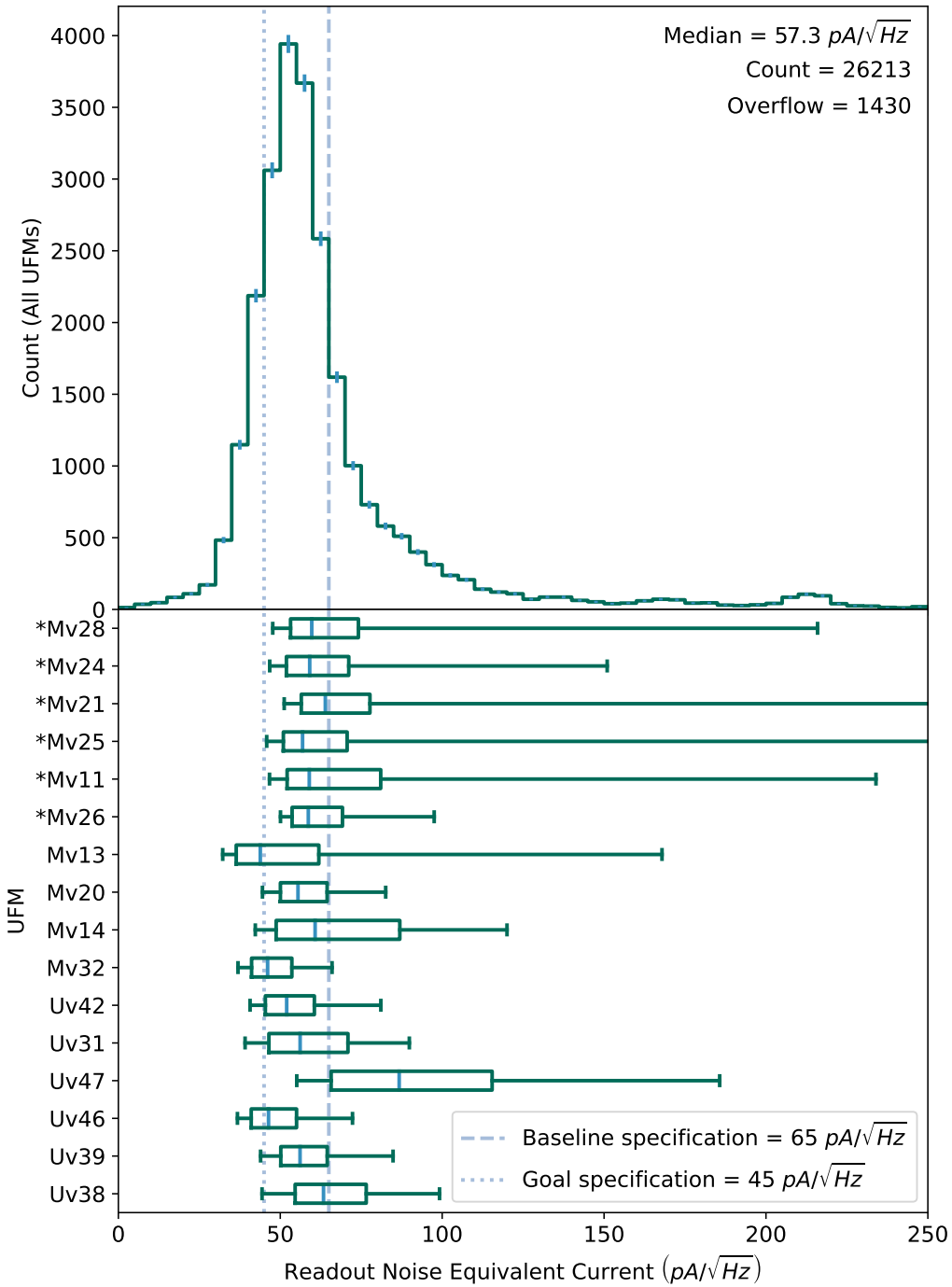


Figure 5: Readout noise equivalent current calculated from time streams with the detectors normal for 16 UFMs. Note that for the UFMs marked with asterisks, the detectors were made normal by driving saturation current down their bias lines, while for the other UFMs, the detectors were made normal by raising the bath temperature above their critical temperatures. Top panel shows the distribution of all detectors on the 16 UFMs, while the bottom panel shows the distribution within each UFM. Boxes show the second and third quartiles of data with medians marked by vertical blue lines, while the whiskers bound the central 80% of data. Vertical dashed and dotted lines show the baseline and goal specifications, respectively.

3. CONCLUSION

These results show promising progress towards commissioning the detectors and readout systems of the Simons Observatory's LAT. While some of the deployed UFM and SMuRF systems are affected by understood readout hardware issues, a large portion of the remaining systems show detector yield and readout noise levels which are consistent with the observatory's baseline specifications for science operation. As we bring the remaining systems online later in 2024, we will employ similar procedures to characterize these systems and ensure their readiness for operation.

ACKNOWLEDGMENTS

This work was supported in part by the Department of Energy, Laboratory Directed Research and Development program at SLAC National Accelerator Laboratory, under contract DE-AC02-76SF00515. This work was also supported in part by a grant from the Simons Foundation (Award #457687, B.K.). This work was also supported by the National Science Foundation (UEI GM1XX56LEP58). Several figures in this paper were created using the Python packages `numpy` and `matplotlib`.¹⁵¹⁶

REFERENCES

- [1] Ade, P., Aguirre, J., Ahmed, Z., Aiola, S., Ali, A., Alonso, D., Alvarez, M. A., Arnold, K., Ashton, P., Austermann, J., Awan, H., Baccigalupi, C., Baildon, T., Barron, D., Battaglia, N., Battye, R., Baxter, E., Bazarko, A., Beall, J. A., Bean, R., Beck, D., Beckman, S., Beringue, B., Bianchini, F., Boada, S., Boettger, D., Bond, J. R., Borrill, J., Brown, M. L., Bruno, S. M., Bryan, S., Calabrese, E., Calafut, V., Calisse, P., Carron, J., Challinor, A., Chesmore, G., Chinone, Y., Chluba, J., Cho, H.-M. S., Choi, S., Coppi, G., Cothard, N. F., Coughlin, K., Crichton, D., Crowley, K. D., Crowley, K. T., Cukierman, A., D'Ewart, J. M., Dünner, R., de Haan, T., Devlin, M., Dicker, S., Didier, J., Dobbs, M., Dober, B., Duell, C. J., Duff, S., Duivenvoorden, A., Dunkley, J., Dusatko, J., Errard, J., Fabbian, G., Feeney, S., Ferraro, S., Fluxà, P., Freese, K., Frisch, J. C., Frolov, A., Fuller, G., Fuzia, B., Galitzki, N., Gallardo, P. A., Ghersi, J. T. G., Gao, J., Gawiser, E., Gerbino, M., Gluscevic, V., Goeckner-Wald, N., Golec, J., Gordon, S., Gralla, M., Green, D., Grigorian, A., Groh, J., Groppi, C., Guan, Y., Gudmundsson, J. E., Han, D., Hargrave, P., Hasegawa, M., Hasselfield, M., Hattori, M., Haynes, V., Hazumi, M., He, Y., Healy, E., Henderson, S. W., Hervias-Caimapo, C., Hill, C. A., Hill, J. C., Hilton, G., Hilton, M., Hincks, A. D., Hinshaw, G., Hložek, R., Ho, S., Ho, S.-P. P., Howe, L., Huang, Z., Hubmayr, J., Huppenberger, K., Hughes, J. P., Ijjas, A., Ikape, M., Irwin, K., Jaffe, A. H., Jain, B., Jeong, O., Kaneko, D., Karpel, E. D., Katayama, N., Keating, B., Kernasovskiy, S. S., Keskitalo, R., Kisner, T., Kiuchi, K., Klein, J., Knowles, K., Koopman, B., Kosowsky, A., Krachmalnicoff, N., Kuenstner, S. E., Kuo, C.-L., Kusaka, A., Lashner, J., Lee, A., Lee, E., Leon, D., Leung, J. S.-Y., Lewis, A., Li, Y., Li, Z., Limon, M., Linder, E., Lopez-Caraballo, C., Louis, T., Lowry, L., Lungu, M., Madhavacheril, M., Mak, D., Maldonado, F., Mani, H., Mates, B., Matsuda, F., Maurin, L., Mauskopf, P., May, A., McCallum, N., McKenney, C., McMahon, J., Meerburg, P. D., Meyers, J., Miller, A., Mirmelstein, M., Moodley, K., Munchmeyer, M., Munson, C., Naess, S., Nati, F., Navaroli, M., Newburgh, L., Nguyen, H. N., Niemack, M., Nishino, H., Orlowski-Scherer, J., Page, L., Partridge, B., Peloton, J., Perrotta, F., Piccirillo, L., Pisano, G., Poletti, D., Puddu, R., Puglisi, G., Raum, C., Reichardt, C. L., Remazeilles, M., Rephaeli, Y., Riechers, D., Rojas, F., Roy, A., Sadeh, S., Sakurai, Y., Salatino, M., Rao, M. S., Schaan, E., Schmittfull, M., Sehgal, N., Seibert, J., Seljak, U., Sherwin, B., Shimon, M., Sierra, C., Sievers, J., Sikhosana, P., Silva-Feaver, M., Simon, S. M., Sinclair, A., Siritanasak, P., Smith, K., Smith, S. R., Spergel, D., Staggs, S. T., Stein, G., Stevens, J. R., Stompor, R., Suzuki, A., Tajima, O., Takakura, S., Teply, G., Thomas, D. B., Thorne, B., Thornton, R., Trac, H., Tsai, C., Tucker, C., Ullom, J., Vagnozzi, S., van Engelen, A., Lanen, J. V., Winkle, D. D. V., Vavagiakis, E. M., Vergès, C., Vissers, M., Wagoner, K., Walker, S., Ward, J., Westbrook, B., Whitehorn, N., Williams, J., Williams, J., Wollack, E. J., Xu, Z., Yu, B., Yu, C., Zago, F., Zhang, H., and Zhu, N., “The Simons Observatory: science goals and forecasts,” *Journal of Cosmology and Astroparticle Physics* **2019**, 056 (feb 2019).
- [2] Galitzki, N., Tsan, T., Spisak, J., Randall, M., Silva-Feaver, M., Seibert, J., Lashner, J., Adachi, S., Adkins, S. M., Alford, T., Arnold, K., Ashton, P. C., Austermann, J. E., Baccigalupi, C., Bazarko, A., Beall, J. A., Bhimani, S., Bixler, B., Coppi, G., Corbett, L., Crowley, K. D., Crowley, K. T., Day-Weiss, S., Dicker, S.,

- Dow, P. N., Duell, C. J., Duff, S. M., Gerras, R. G., Groh, J. C., Gudmundsson, J. E., Harrington, K., Hasegawa, M., Healy, E., Henderson, S. W., Hubmayr, J., Iuliano, J., Johnson, B. R., Keating, B., Keller, B., Kiuchi, K., Kofman, A. M., Koopman, B. J., Kusaka, A., Lee, A. T., Lew, R. A., Lin, L. T., Link, M. J., Lucas, T. J., Lungu, M., Mangu, A., McMahon, J. J., Miller, A. D., Moore, J. E., Morshed, M., Nakata, H., Nati, F., Newburgh, L. B., Nguyen, D. V., Niemack, M. D., Page, L. A., Sakaguri, K., Sakurai, Y., Rao, M. S., Saunders, L. J., Shroyer, J. E., Sugiyama, J., Tajima, O., Takeuchi, A., Bua, R. T., Teply, G., Terasaki, T., Ullom, J. N., Lanen, J. L. V., Vavagiakis, E. M., Vissers, M. R., Walters, L., Wang, Y., Xu, Z., Yamada, K., and Zheng, K., “The Simons Observatory: Design, integration, and testing of the small aperture telescopes,” (2024).
- [3] Zhu, N., Bhandarkar, T., Coppi, G., Kofman, A. M., Orłowski-Scherer, J. L., Xu, Z., Adachi, S., Ade, P., Aiola, S., Austermann, J., Bazarko, A. O., Beall, J. A., Bhimani, S., Bond, J. R., Chesmore, G. E., Choi, S. K., Connors, J., Cothard, N. F., Devlin, M., Dicker, S., Dober, B., Duell, C. J., Duff, S. M., Dünner, R., Fabbian, G., Galitzki, N., Gallardo, P. A., Golec, J. E., Haridas, S. K., Harrington, K., Healy, E., Ho, S.-P. P., Huber, Z. B., Hubmayr, J., Iuliano, J., Johnson, B. R., Keating, B., Kiuchi, K., Koopman, B. J., Lashner, J., Lee, A. T., Li, Y., Limon, M., Link, M., Lucas, T. J., McCarrick, H., Moore, J., Nati, F., Newburgh, L. B., Niemack, M. D., Pierpaoli, E., Randall, M. J., Sarmiento, K. P., Saunders, L. J., Seibert, J., Sierra, C., Sonka, R., Spisak, J., Sutariya, S., Tajima, O., Teply, G. P., Thornton, R. J., Tsan, T., Tucker, C., Ullom, J., Vavagiakis, E. M., Vissers, M. R., Walker, S., Westbrook, B., Wollack, E. J., and Zannoni, M., “The Simons Observatory large aperture telescope receiver,” *The Astrophysical Journal Supplement Series* **256**, 23 (sep 2021).
- [4] McCarrick, H., Healy, E., Ahmed, Z., Arnold, K., Atkins, Z., Austermann, J. E., Bhandarkar, T., Beall, J. A., Bruno, S. M., Choi, S. K., Connors, J., Cothard, N. F., Crowley, K. D., Dicker, S., Dober, B., Duell, C. J., Duff, S. M., Dutcher, D., Frisch, J. C., Galitzki, N., Gralla, M. B., Gudmundsson, J. E., Henderson, S. W., Hilton, G. C., Ho, S.-P. P., Huber, Z. B., Hubmayr, J., Iuliano, J., Johnson, B. R., Kofman, A. M., Kusaka, A., Lashner, J., Lee, A. T., Li, Y., Link, M. J., Lucas, T. J., Lungu, M., Mates, J. A. B., McMahon, J. J., Niemack, M. D., Orłowski-Scherer, J., Seibert, J., Silva-Feaver, M., Simon, S. M., Staggs, S., Suzuki, A., Terasaki, T., Thornton, R., Ullom, J. N., Vavagiakis, E. M., Vale, L. R., Lanen, J. V., Vissers, M. R., Wang, Y., Wollack, E. J., Xu, Z., Young, E., Yu, C., Zheng, K., and Zhu, N., “The Simons Observatory microwave SQUID multiplexing detector module design,” *The Astrophysical Journal* **922**, 38 (nov 2021).
- [5] Mates, J. A. B., *The microwave SQUID multiplexer*, PhD thesis, University of Colorado (2011).
- [6] Dober, B., Ahmed, Z., Arnold, K., Becker, D. T., Bennett, D. A., Connors, J. A., Cukierman, A., D’Ewart, J. M., Duff, S. M., Dusatko, J. E., Frisch, J. C., Gard, J. D., Henderson, S. W., Herbst, R., Hilton, G. C., Hubmayr, J., Li, Y., Mates, J. A. B., McCarrick, H., Reintsema, C. D., Silva-Feaver, M., Ruckman, L., Ullom, J. N., Vale, L. R., Van Winkle, D. D., Vasquez, J., Wang, Y., Young, E., Yu, C., and Zheng, K., “A microwave SQUID multiplexer optimized for bolometric applications,” *Applied Physics Letters* **118**, 062601 (02 2021).
- [7] Montgomery, J., Ade, P. A. R., Ahmed, Z., Anderes, E., Anderson, A. J., Archipley, M., Avva, J. S., Aylor, K., Balkenhol, L., Barry, P. S., Thakur, R. B., Benabed, K., Bender, A. N., Benson, B. A., Bianchini, F., Bleem, L. E., Bouchet, F. R., Bryant, L., Byrum, K., Carlstrom, J. E., Carter, F. W., Cecil, T. W., Chang, C. L., Chaubal, P., Chen, G., Cho, H., Chou, T.-L., Cliche, J.-F., Crawford, T. M., Cukierman, A., Daley, C., de Haan, T., Denison, E. V., Dibert, K., Ding, J., Dobbs, M. A., Dutcher, D., Elleflot, T., Everett, W., Feng, C., Ferguson, K. R., Foster, A., Fu, J., Galli, S., Gambrel, A. E., Gardner, R. W., Goeckner-Wald, N., Groh, J. C., Gualtieri, R., Guns, S., Gupta, N., Guysler, R., Halverson, N. W., Harke-Hosemann, A. H., Harrington, N. L., Henning, J. W., Hilton, G. C., Hivon, E., Holzappel, W. L., Hood, J. C., Howe, D., Huang, N., Irwin, K. D., Jeong, O. B., Jonas, M., Jones, A., Khaire, T. S., Knox, L., Kofman, A. M., Korman, M., Kubik, D. L., Kuhlmann, S., Kuo, C.-L., Lee, A. T., Leitch, E. M., Lowitz, A. E., Lu, C., Meyer, S. S., Michalik, D., Millea, M., Nadolski, A., Natoli, T., Nguyen, H., Noble, G. I., Novosad, V., Omori, Y., Padin, S., Pan, Z., Paschos, P., Pearson, J., Posada, C. M., Prabhu, K., Quan, W., Rahlin, A., Reichardt, C. L., Riebel, D., Riedel, B., Rouble, M., Ruhl, J. E., Sayre, J. T., Schiappucci, E., Shirokoff, E., Smecher, G., Sobrin, J. A., Stark, A. A., Stephen, J., Story, K. T., Suzuki, A., Thompson, K. L., Thorne, B., Tucker, C., Umiltà, C., Vale, L. R., Vanderlinde, K., Vieira, J. D., Wang, G., Whitehorn, N., Wu, W. L. K., Yefremenko, V., Yoon, K. W., and Young, M. R., “Performance and characterization of the SPT-3G digital

frequency-domain multiplexed readout system using an improved noise and crosstalk model,” *Journal of Astronomical Telescopes, Instruments, and Systems* **8** (Jan. 2022).

- [8] Duff, S., Austermann, J., Beall, J., Daniel, D., Hubmayr, J., Jaehnig, G., Johnson, B., Jones, D., Link, M., Lucas, T., Sonka, R., Staggs, S., Ullom, J., and Wang, Y., “The Simons Observatory: Production-level fabrication of the mid- and ultra-high-frequency wafers,” *Journal of Low Temperature Physics*, 1–9 (05 2024).
- [9] Jones, D., Singh, R., Austermann, J., Beall, J., Daniel, D., Duff, S., Dutcher, D., Groh, J., Hubmayr, J., Johnson, B., Lew, R., Link, M., Lucas, T., Mates, J., Staggs, S., Ullom, J., Vale, L., Van Lanen, J., Vissers, M., and Wang, Y., “Qualification of microwave SQUID multiplexer chips for Simons Observatory,” *Journal of Low Temperature Physics* (2024). Publisher Copyright: © The Author(s) 2024.
- [10] Yu, C., Ahmed, Z., Frisch, J. C., Henderson, S. W., Silva-Feaver, M., Arnold, K., Brown, D., Connors, J., Cukierman, A. J., D’Ewart, J. M., Dober, B. J., Dusatko, J. E., Haller, G., Herbst, R., Hilton, G. C., Hubmayr, J., Irwin, K. D., Kuo, C.-L., Mates, J. A. B., Ruckman, L., Ullom, J., Vale, L., Van Winkle, D. D., Vasquez, J., and Young, E., “SLAC microresonator RF (SMuRF) electronics: A tone-tracking readout system for superconducting microwave resonator arrays,” *Review of Scientific Instruments* **94**, 014712 (01 2023).
- [11] Dicker, S. R., Ade, P. A. R., Aguirre, J., Brevik, J. A., Cho, H. M., Datta, R., Devlin, M. J., Dober, B., Egan, D., Ford, J., Ford, P., Hilton, G., Hubmayr, J., Irwin, K. D., Mason, B. S., Marganian, P., Mello, M., McMahon, J. J., Mroczkowski, T., Romero, C., Stanchfield, S., Tucker, C., Vale, L., White, S., Whitehead, M., and Young, A. H., “MUSTANG2: a large focal plan array for the 100 meter Green Bank Telescope,” in [*Millimeter, Submillimeter, and Far-Infrared Detectors and Instrumentation for Astronomy VII*], Holland, W. S. and Zmuidzinas, J., eds., **9153**, 91530J, International Society for Optics and Photonics, SPIE (2014).
- [12] Cukierman, A., Ahmed, Z., Henderson, S., Young, E., Yu, C., Barkats, D., Brown, D., Chaudhuri, S., Cornelison, J., D’Ewart, J. M., Dierickx, M., Dober, B. J., Dusatko, J., Fatigoni, S., Filippini, J. P., Frisch, J. C., Haller, G., Halpern, M., Hilton, G. C., Hubmayr, J., Irwin, K. D., Karkare, K. S., Karpel, E., Kernasovskiy, S. A., Kovac, J. M., Kovacs, A., Kuenstner, S. E., Kuo, C. L., Li, D., Mates, J. A. B., Smith, S., St. Germaine, T., Ullom, J. N., Vale, L. R., Van Winkle, D. D., Vasquez, J., Willmert, J., Zeng, L., Ade, P. A. R., Amiri, M., Basu Thakur, R., Bischoff, C. A., Bock, J. J., Boenish, H., Bullock, E., Buza, V., Cheshire, J., Connors, J., Crumrine, M., Duband, L., Hall, G., Harrison, S., Hildebrandt, S. R., Hui, H., Kang, J., Kefeli, S., Lau, K., Megerian, K. G., Moncelsi, L., Namikawa, T., Nguyen, H. T., O’Brien, R., Palladino, S., Pryke, C., Racine, B., Reintsema, C. D., Richter, S., Schillaci, A., Schwarz, R., Sheehy, C. D., Soliman, A., Steinbach, B., Sudiwala, R. V., Thompson, K. L., Tucker, C., Turner, A. D., Umiltà, C., Vieregg, A. G., Wandui, A., Weber, A. C., Wiebe, D. V., Wu, W. L. K., Yang, H., Yoon, K. W., and Zhang, C., “Microwave multiplexing on the Keck array,” *Journal of Low Temperature Physics* **199**, 858–866 (Dec. 2019).
- [13] Dutcher, D., Duff, S. M., Groh, J. C., Healy, E., Hubmayr, J., Johnson, B. R., Jones, D., Keller, B., Lin, L. T., Link, M. J., Lucas, T. J., Morgan, S., Seino, Y., Sonka, R. F., Staggs, S. T., Wang, Y., and Zheng, K., “The Simons Observatory: Large-scale characterization of 90/150 GHz TES detector modules,” (Nov. 2023).
- [14] Healy, E., Dutcher, D., Atkins, Z. R., Austermann, J., Choi, S. K., Duell, C. J., Duff, S. M., Galitzki, N., Huber, Z. B., Hubmayr, J., Johnson, B. R., McCarrick, H., Niemack, M. D., Sonka, R. F., Staggs, S. T., Vavagiakis, E. M., Wang, Y., Xu, Z., and Zheng, K., “The Simons Observatory 220 and 280 GHz focal-plane module: Design and initial characterization,” *Journal of Low Temperature Physics* **209**, 815 – 823 (2022).
- [15] Harris, C. R., Millman, K. J., van der Walt, S. J., Gommers, R., Virtanen, P., Cournapeau, D., Wieser, E., Taylor, J., Berg, S., Smith, N. J., Kern, R., Picus, M., Hoyer, S., van Kerkwijk, M. H., Brett, M., Haldane, A., del Río, J. F., Wiebe, M., Peterson, P., Gérard-Marchant, P., Sheppard, K., Reddy, T., Weckesser, W., Abbasi, H., Gohlke, C., and Oliphant, T. E., “Array programming with NumPy,” *Nature* **585**, 357–362 (Sept. 2020).
- [16] Hunter, J. D., “Matplotlib: A 2d graphics environment,” *Computing in Science & Engineering* **9**(3), 90–95 (2007).